Quantum Science and Technology

PAPER

Microscopic 3D printed optical tweezers for atomic quantum technology

Pavel Ruchka[1,4], Sina Hammer[2,4], Marian Rockenhäuser[2], Ralf Albrecht[2], Johannes Drozella[3], Simon Thiele[3], Harald Giessen[1] and Tim Langen[2,*]

[1] 4. Physikalisches Institut, Research Center SCoPE and Center for Integrated Quantum Science and Technology, Universität Stuttgart, Pfaffenwaldring 57, 70569 Stuttgart, Germany
[2] 5. Physikalisches Institut and Center for Integrated Quantum Science and Technology, Universität Stuttgart, Pfaffenwaldring 57, 70569 Stuttgart, Germany
[3] Institute of Applied Optics (ITO) and Research Center SCoPE, University of Stuttgart, Pfaffenwaldring 9, 70569 Stuttgart, Germany
[*] Author to whom any correspondence should be addressed.
[4] These two authors contributed equally.

E-mail: t.langen@physik.uni-stuttgart.de

Keywords: optical tweezers, ultracold atoms, 3D printing

OPEN ACCESS

RECEIVED
15 March 2022

REVISED
4 June 2022

ACCEPTED FOR PUBLICATION
16 June 2022

PUBLISHED
20 July 2022

Original content from this work may be used under the terms of the Creative Commons Attribution 4.0 licence.

Any further distribution of this work must maintain attribution to the author(s) and the title of the work, journal citation and DOI.

Abstract

Trapping of single ultracold atoms is an important tool for applications ranging from quantum computation and communication to sensing. However, most experimental setups, while very precise and versatile, can only be operated in specialized laboratory environments due to their large size, complexity and high cost. Here, we introduce a new trapping concept for ultracold atoms in optical tweezers based on micrometer-scale lenses that are 3D printed onto the tip of standard optical fibers. The unique properties of these lenses make them suitable for both trapping individual atoms and capturing their fluorescence with high efficiency. In an exploratory experiment, we have established the vacuum compatibility and robustness of the structures, and successfully formed a magneto-optical trap for ultracold atoms in their immediate vicinity. This makes them promising components for portable atomic quantum devices.

1. Introduction

Starting from the early landmark work on the trapping of dielectric particles [1, 2], optical tweezer traps have matured into one of the key technologies for the manipulation of single, ultracold atoms in quantum science and technology [3]. Applications range from quantum simulation [4–7] and computing [8–10] to studies of fundamental chemical processes and collisions [11–13], precision timekeeping [14, 15], interfacing with nanophotonic structures [16, 17] and single-photon generation [18].

However, experimental setups combining optical tweezers and ultracold atoms typically have macroscopic dimensions, are complex, and require sophisticated calibration and stable laboratory environments. In order to realize more compact, robust, and user-friendly technological applications, it is thus highly desirable to simplify and further miniaturize these setups.

Here, we introduce a new optical tweezer concept for ultracold atoms that can meet these requirements. Our approach is based on microscopic lenses that are 3D printed on the tip of optical fibers. Similar 3D printed structures have already been used to realize a diverse range of optical components from endoscopes [19] to multi-lens objectives [20]. This enabled the realization of tweezer traps for classical microscopic objects in chemical and biological environments [21, 22], large-size microlens arrays [23] and the coupling of single quantum dot emission into an optical fiber [24]. In the following, we establish that these micrometer-sized structures are also well suited to manipulate ultracold atoms inside an ultrahigh vacuum environment. In particular, due to the large flexibility afforded by the 3D printing, it will be possible to integrate single-atom trapping *and* high-fidelity detection into a single, compact device.

© 2022 The Author(s). Published by IOP Publishing Ltd

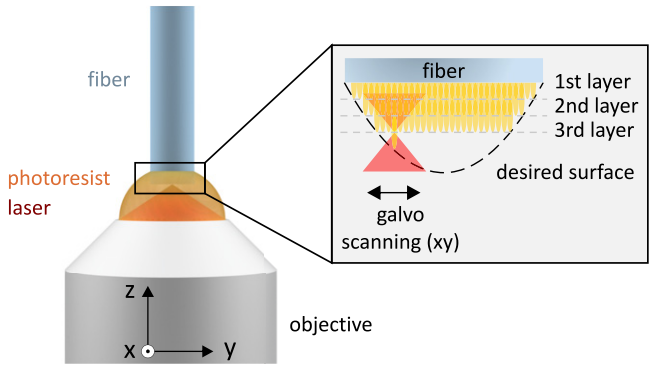

Figure 1. Schematic representation of the printing process using two-photon polymerization. We use a dip-in method, where a drop of photoresist is placed onto a microscope objective. The fiber is then dipped into this drop and a single voxel of the final structure is created in the focal spot of a high-power writing laser. Arbitrary structures are constructed layer by layer from many individual voxels, by scanning the laser focus position both laterally (*xyz*) using a galvo scanner and vertically (*z*) by displacing the objective.

2. Fabrication

3D printing has revolutionized many areas of research, engineering and production, making it one of the most significant inventions of recent years [25]. With the existing techniques it is possible to produce individually designed objects from a large variety of materials, with sizes ranging from micro- to macro-scales [26–31].

3D printing of micrometer-sized optical components is possible using two-photon polymerization [32–35]. In this technique, the desired structures are directly written into a photoresist using a focused laser beam (figure 1). For the printing of microscopic fiber lenses, we use negative photoresists, which polymerize after exposure [36]. The focal spot of the laser beam defines the smallest building block of any solid structure formed in this way. This smallest unit is commonly referred to as a *voxel*.

We use a commercially available 3D printer [Nanoscribe Professional GT (Nanoscribe GmbH)], together with a pulsed femtosecond laser at 780 nm and pulse powers of around 2.25 nJ to realize voxels with dimensions down to 100 nm. This minimum voxel size sets the scale for the design of any larger structures [19].

The lenses are then built sequentially out of such voxels using a dip-in laser lithography configuration. In this configuration, the photoresist is directly placed onto the objective for the writing laser. For the writing process, a cleaved and oxygen plasma-activated fiber is dipped into the resist and the laser focus position is scanned using two galvo-mirrors and piezo actuators that move the objective. We increase the adhesion of the printed structure to the fiber by silanizing the substrate [37]. To precisely align the fiber, the writing laser is attenuated and its position on the fiber is tracked using a charge-coupled device (CCD) camera. After writing, the micro-optics are developed by placing them in a bath with developer [Micro Resist Technology mr-Dev600] for 15 min and by rinsing them with a solvent. This dissolves the non-exposed parts of the negative photoresist to reveal the final, printed structure. Finally, the micro-optics are UV-cured, which ensures full polymerization and, as a consequence, consistency of the refractive index.

The specific geometries of the lenses are designed using optical ray tracing [Zemax OpticStudio] and wave propagation method (WPM) simulations [38, 39]. Subsequently, the designs are translated into trajectories for the writing process. In this process, the mechanical configuration of the printing setup facilitates precise control of the voxel position in three dimensions. This allows us to adjust parameters like the voxel layer thickness along the fiber axis, as well as the distance between two layers in one printing plane according to the optical design of the desired structure and photoresist type. The resolution of the overall process is given by an interplay of several parameters, which include the magnification and numerical aperture (NA) of the objective, photopolymer characteristics, laser power, scanning speed and the precision of the optomechanical parts, such as galvo mirrors and positioning stages. As we demonstrate in the following, taking all of these aspects into account, we are able to closely reproduce the initial optical designs.

3. Example designs

The goal of our concept is to form an optical tweezer by guiding light through a single mode optical fiber and focusing it down using the 3D printed optics. At the same time, resonant fluorescence emitted by atoms

Table 1. Parameters of the fiber lens examples presented in this work. The chromatic focal shift is given between the two wavelength of interest: 1064 and 780 nm. The working distance is given for 1064 nm and refers to the closest distance between the lens structures and the focal point (see figures 2 and 3 for reference).

Lens type	Aspheric	Aspheric	TIR
Numerical aperture	0.45	0.6	0.75
Focal spot diameter	2 μm	1.5 μm	1.4 μm
Working distance	83.3 μm	36.2 μm	46.3 μm
Chromatic focal shift	-1.1 μm	-0.4 μm	-1.6 μm
Solid angle covered	4.83%	9%	15%

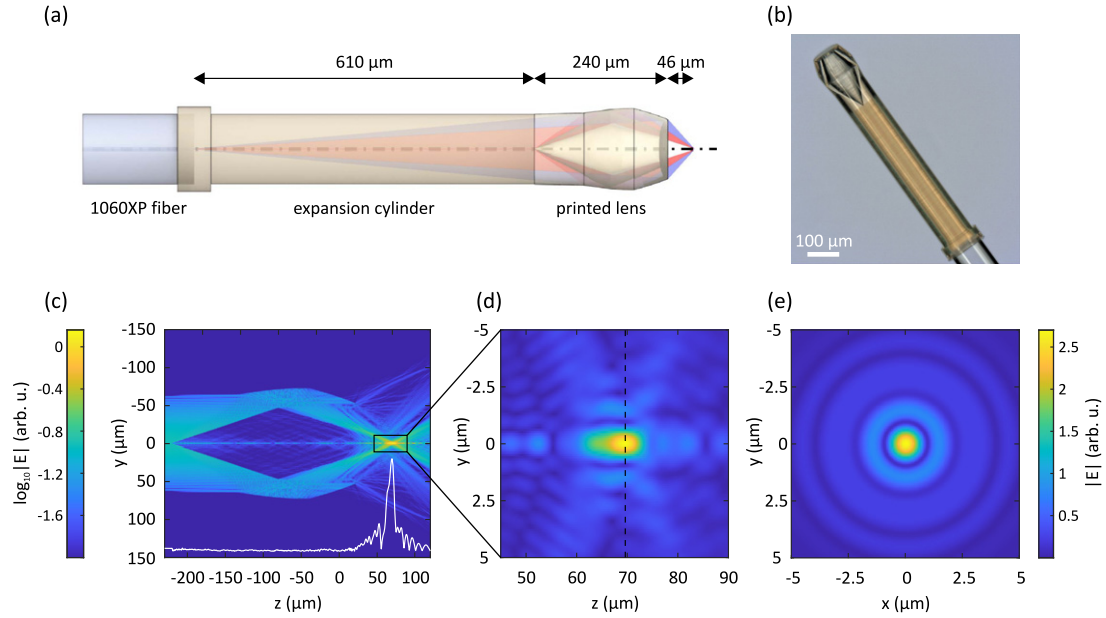

Figure 2. TIR lens design. A sketch of the design is depicted in (a), highlighting the reflective, rather than diffractive nature of the design. (b) displays the printed lens structure under a microscope. In (c) the WPM-simulated electric field is shown on a logarithmic color scale. The white line is a cut along z through the origin ($y = 0$). The inset (d) corresponds to a zoom into the focal region of this simulation, revealing a high quality focal spot, with a $1/e$ diameter of 1.4 μm. (e) is the radial cross-section at the focal spot, as indicated by the dashed line in (d). The latter two panels are plotted using a linear color-scale.

trapped in the tweezer is to be collected using the printed optics and, after separation from the incoming trapping light, guided towards a photodetector.

Different approaches for the lens design are possible to realize this configuration. For the creation of a tweezer trap and, subsequently, efficient detection of the atomic fluorescence, a lens with a high NA is desirable. In the following, we present three examples for suitable lenses. Their key properties are summarized in table 1. Due to the flexibility afforded by the 3D printing process, many others—tailored to meet specific requirements—are conceivable.

3.1. Total-internal reflection design

As a first example, we present a lens based on a total-internal reflection design (TIR), which is shown in figure 2. A similar design has previously been used to trap μm sized particles in water [22].

To realize small foci suitable for single-atom trapping [40], the light from the fiber is first expanded through a 610 μm long printed cylinder before subsequently passing through the lens. The lens itself uses fully reflective, rather than standard refractive optics, to achieve an NA of 0.75 and a working distance of 46.3 μm. Larger NAs approaching unity are possible at the expense of a shorter working distance. One crucial benefit of such a lens for the work with ultracold atoms is the combination of a high NA with a large working distance, as can be seen by comparing it to more conventional designs with similar NA (see table 1). Additionally, the lens design could be optimized to achieve even lower chromatic focal shifts due to its reflective nature.

We simulate the resulting field using WPM simulations and find a high-quality focal spot with a $1/e$ diameter of 1.4 μm. Printing is realized using commercially available Nanoscribe IP-Dip resist and takes approximately 5 h including the expansion cylinder.

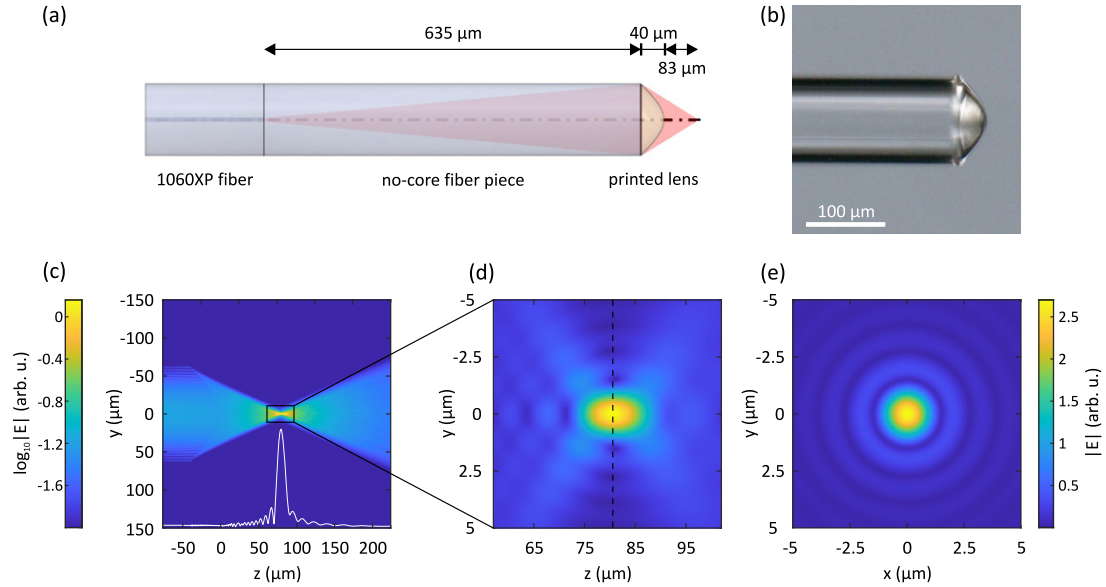

Figure 3. Aspherical lens design. (a) Sketch of the design for NA = 0.45. (b) Microscope image of the corresponding lens. (c) WPM-simulations of the electric field, plotted using a logarithmic color-scale for clarity. The white line is a cut along z through the origin ($y = 0$). (d) Zoom into the focal region, with a $1/e$ diameter of 2 μm. (e) is the radial cross-section at the focal spot, as indicated by the dashed line in (d). The latter two panels are plotted using a linear color-scale.

3.2. Aspheric design

As a next example, we realize two types of aspheric lenses. Aspheric lenses are another possibility to achieve a high-quality focal spot using small-scale optics without the use of objectives containing multiple lenses.

For our designs, we first expand the beam from a single-mode fiber in a 635 μm long expansion cylinder formed by a piece of no-core fiber that is spliced to the single-mode fiber. Subsequently, we focus down the beam using the respective 3D printed aspheric lens. Compared to the printed expansion cylinder this approach enables much faster production. The additional refraction at the cylinder-lens interface can be neglected for the design of the simple aspheric lenses. In principle, a similar approach could also be taken for the TIR optics discussed above, but due to angle mismatches that can be caused by the interface, this would require a more extensive optimization.

With the first lens design a NA of 0.45 and a working distance of 83.3 μm are realized (see figure 3). The second lens follows the same design principles and is characterized by an NA of 0.6 and a working distance of 36.2 μm. We find focal spots with $1/e$ diameters of 2 μm and 1.5 μm, respectively.

This highlights that the aspheric singlet design is an effective tool to create a small foci at a particular distance. However, while this solution is easy to design, simulate and implement, it has some limitations due to its refractive nature. For instance, the interdependence of NA, working distance and the size of the focal spot makes it challenging to create small foci at a higher distance, when one is limited by a 125 μm fiber diameter. However, it is possible to splice a no-core fiber with a larger diameter (e.g., 250 μm), which would allow for an increase of the working distance, while maintaining the relatively high NA and tight focusing.

As the structure of both aspheric designs is comparably simple, printing using Nanoscribe IP-S resist can be achieved in less than an hour for both of them. Compared to the IP-Dip resist used for the TIR lens, IP-S allows achieving smoother surfaces, which is of a special importance when printing the refractive aspheric optics.

3.3. Detection efficiency

To ensure that the fluorescence emitted by the atoms trapped in the focal spot can be collected and coupled back into the fiber, the focal spots for the different wavelengths used for trapping and fluorescence detection must be precisely matched. In the following, we will use rubidium atoms as an example, where fluorescence is emitted at 780 nm and a typical, far-detuned trapping wavelength is 1064 nm. All designs can easily be adjusted to cover also the wavelengths for a large variety of other atomic and molecular species.

We theoretically investigate the behavior of both lens designs by considering a trapped atom as a perfect source radiating uniformly in all directions and reversing the optical system using ray tracing software [Zemax OpticStudio]. Independent of the lens design we find that the focal spots for 1064 nm and 780 nm are displaced by 1–2 μm, and thus located exceptionally close to each other. The lenses thus cover between

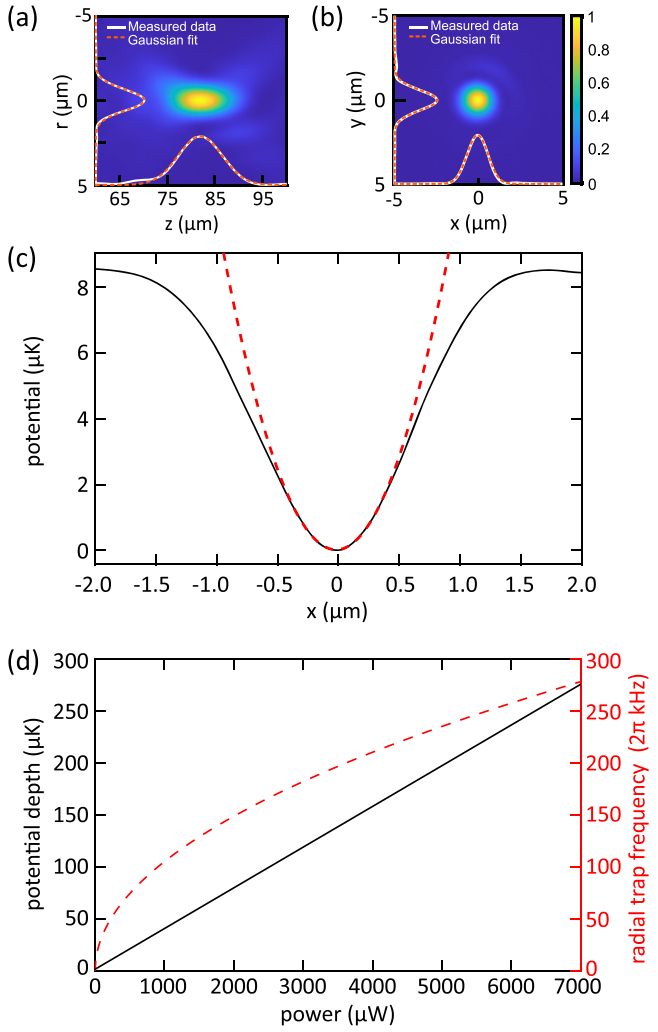

Figure 4. Measurements of the focal spot of the aspherical lens design with NA = 0.45 along the laser beam axis (a) and perpendicular to it (b). Colors denote the normalized intensity. For this measurement, the power exiting the fiber was 220 μW. The result is in excellent agreement with the corresponding simulation shown in figures 3(d) and (e). (c) Exemplary trapping potential along the perpendicular axis deduced from these measurements using equation (1). The red dashed line is a harmonic fit, which yields a radial trapping frequency of approximately $\omega = 2\pi \times 73$ kHz. The trapping potential shown is a cut along the horizontal dotted line. (d) Potential depth (solid black line) and radial trapping frequency (red dashed line) as a function of the power exiting the fiber.

5.4% to 17% of the solid angle of a trapped particle. As mentioned above, in principle, NAs of up to 0.99 are possible, corresponding to detection efficiencies that can well exceed 40%.

Another important aspect for the detection efficiency of single trapped atoms are spurious photons that are created in the fiber or the polymer [18]. Monitoring the output of the fibers with single-photon counters we have not observed any Raman shifted light at 780 nm from a 1064 nm laser beam for input powers up to 100 mW. We therefore expect the fluorescence detection based on the fiber lenses to be suitable down to the single-atom and single-photon level, even in the presence of significant powers for the realization of the tweezer trap.

3.4. Focal spot quality and trapping potentials

We experimentally confirm our simulations, the optical properties of the fiber lenses and the quality of the 3D printing process using through-focus measurements.

An example, based on the aspherical lens design with NA = 0.45, is shown in figures 4(a) and (b). We find excellent agreement between our simulations and measurements, both in terms of working distance and focal spot, with a deviation of less than 2% from the initial design.

In figures 4(c) and (d), we further use this measurement to estimate the expected trapping potentials experienced by the atoms for a given input laser power.

For alkali atoms, such as rubidium, the trapping potential $V(\mathbf{r})$ in a far-detuned tweezer trap can be approximated by a semi-classical model [41]. This yields

$$V(\mathbf{r}) = \frac{3\pi c^2}{2\omega_0^3}\frac{\Gamma}{\Delta}I(\mathbf{r}), \tag{1}$$

where ω_0 is the atomic transition frequency, Γ is the atomic linewidth, Δ is the detuning of the trapping light from the atomic transition, c denotes the speed of light, and $I(\mathbf{r})$ is the position-dependent intensity distribution created by the fiber lens. For red detuning ($\Delta < 0$) the dipole force $\mathbf{F} = -\nabla V(\mathbf{r})$ attracts atom towards the high intensity focal region. In our example system, rubidium, the remaining parameters are given by $\omega_0 \sim 2\pi \times 384$ THz, corresponding to a wavelength of 780 nm, $\Gamma = 2\pi \times 6$ MHz, and $\Delta \sim 2\pi \times 100$ THz for trapping light at 1064 nm [42]. Trapping potentials for more complex atoms with significant vector and tensor polarizabilities can be derived in a similar way, by combining vector WPM methods for the electric fields with precisely known data for the polarizabilities [43–45].

Based on this, we find that already moderate input laser powers on the order of a few milliwatts generate traps that are hundreds of microkelvins deep, and thus sufficient to capture atoms from a typical magneto-optical trap (MOT). We analyze the trapping potentials further by extracting their characteristic frequencies from a harmonic approximation at the trap center. The results are on the order of hundreds of kHz. We conclude that the very small trapping volume and steep traps are well suited to realize sub-Poissonian loading of single atoms via light-induced collisions [40].

4. Compatibility with ultracold atom technology

To establish the compatibility of the printed structures with ultracold atom technology, we demonstrate the operation of a MOT near the printed structures. This allows us to specifically test several crucial aspects of our concept:

- First, the operation of a MOT and the subsequent stable trapping of single atoms in the tweezer traps place stringent requirements on the vacuum, with pressures that must be well below 1×10^{-7} mbar. It is thus crucial to establish that no significant out-gassing of the polymers and adhesives used in the manufacturing process takes place. Moreover, for more complex designs, like the TIR lens discussed above, virtual leaks from the volume between the faces must be ruled out.
- Second, previous applications of the fiber technology did mostly take place in liquids or in air [21]. In other cases, e.g., when the devices where used for endoscopic applications in medicine, the optics where shielded with a sheath or a cover [19]. On the other hand, alkali atoms are known to strongly corrode many materials. The durability of the structures under long-term exposure to alkali vapors thus has to be established.
- Third, for technological applications the fiber lenses need to be robust enough to remain attached to the fibers even during vacuum pumpdown, a transport of the experimental setup or other vibrations.

Our experimental apparatus to perform these tests consists of a 6 inch stainless steel cube that is permanently pumped by a 50 l s^{-1} ion pump to reach a steady-state pressure of approximately 10^{-9} mbar without any baking. These vacuum conditions are maintained over several months of operation, with no detectable degradation, outgassing or leaking. Six viewports are used to provide optical access for the laser beams required to form a MOT of ^{85}Rb.

The fibers are installed under an angle of 22 degrees relative to the vertical beam axis of the vacuum chamber, with their fiber tips including the micro-optics positioned in the center of the chamber (see figure 5(a)). A standard Swagelok fitting in combination with a Teflon ferrule is used to feed the fiber into vacuum [46]. The inner diameter of the Teflon ferrule is 300 μm in diameter, such that the 125 μm diameter fiber can simply pulled through the ferrule before inserting it into the Swagelok fitting and the chamber. We observe no indication that the pressure in the vacuum chamber is affected by the presence of the various fiber trap designs.

To test the interaction of the fiber with highly-reactive alkali vapors, we intentionally expose the fibers to high rubidium pressures over several hours. We do not observe any influence of this on the optics, except for a thin layer of rubidium oxide forming after removing the fiber from the vacuum chamber figure 5(c).

The printed structures are further robust against vibrations during mounting and operation of the experiment. To test this, the experimental setup was moved several times on a conventional, undamped table, through elevators, up steps and between rooms without air conditioning. Despite significant vibrations with short-term linear accelerations of up to 20 m s^{-2} and significant temperature changes, the lenses remain perfectly attached to the fibers and no negative effect on their optical performance could be observed.

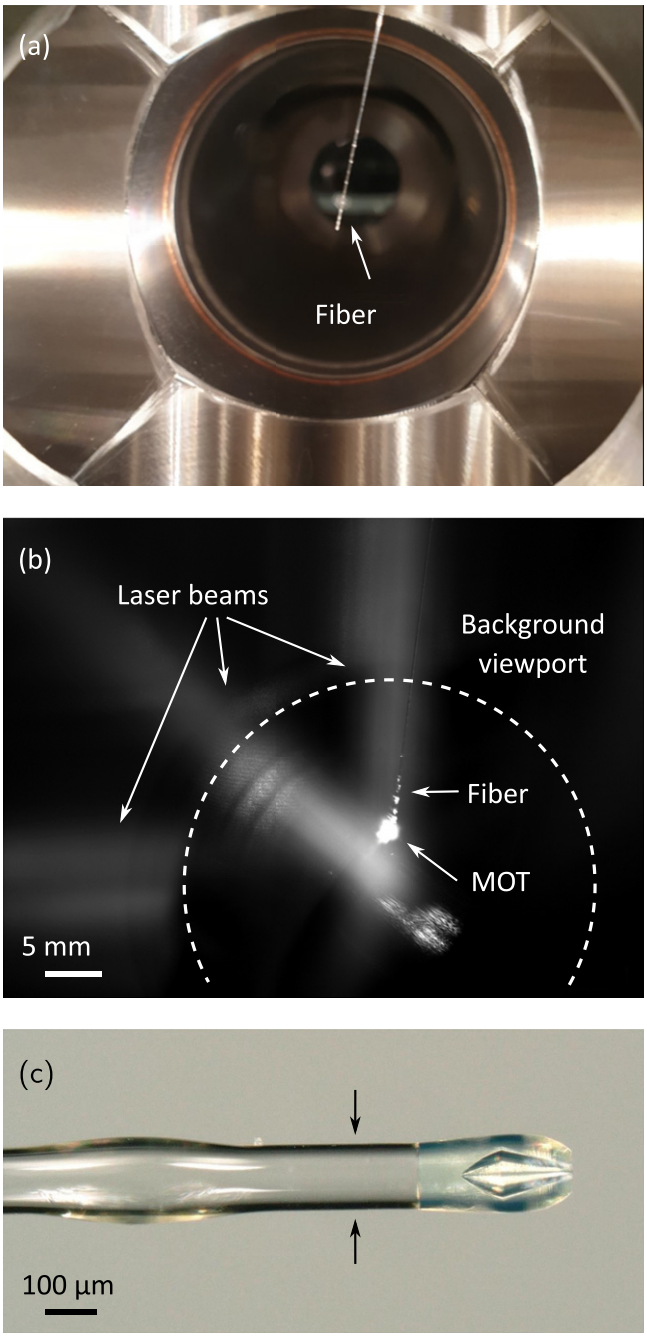

Figure 5. (a) Positioning of the fiber trap in the center of a UHV chamber. (b) Creation of a MOT ∼125 μm from the fiber tip. (c) TIR lens and fiber tip after continuous long-term exposure to high-pressure rubidium vapor, and subsequent removal from the vacuum chamber. The arrow mark a faint black coating that is due to rubidium oxide. Test images similar to the ones shown in figures 4(a) and (b) confirm that this does not affect the performance of the lens.

Finally, we realize magneto-optical trapping of ultracold atoms near the fiber tip. The trap is a macroscopic six-beam MOT, operated with a gradient of 10 G cm^{-1} and combined cooling and repumping laser powers of approximately 1.4 mW per 6 mm diameter beam. Its position relative to the tip of the fiber can be manipulated using additional offset coils. We observe this position by imaging the atomic fluorescence using two CCD cameras positioned perpendicular to each other, and rotated by 45 degrees with respect to the MOT beam axes. With this, we determine that we successfully trap approximately 10^6 atoms, at temperatures close to the Doppler limit, and with the center of the MOT located around 125 μm from the room temperature fiber tip (see figure 5(b)).

5. Conclusion and outlook

We have introduced a new optical tweezer concept based on tailored, 3D printed lenses on the tip of optical fibers. The lenses are of microscopic dimensions, flexible in their design, UHV compatible and robust.

As a next step, we will demonstrate the entire procedure from the dipole trapping of single atoms to their manipulation in the tweezer trap. Currently, background light scatter from the large-diameter laser beams used for the demonstration of the macroscopic MOT renders the detection of single trapped atoms in the fiber trap challenging. This limitation can be fully overcome using integrated and miniaturized setups for ultracold atoms [47, 48].

Our approach integrates particularly well with microfabricated chip, grating and pyramidal MOT assemblies [49–52] and atom chips [53, 54]. We also expect it to be useful for optical manipulation in light-sensitive areas, such as for atoms inside cryostats [55–58], in space applications [59, 60], as well as inside high-field regions with restricted optical access, as required e.g. for certain types of precision measurements [61, 62]. It will further be interesting to combine the approach with additive manufacturing techniques for cold atom setups [28, 63].

A benchmark application of such a microscopic setup will be the realization of a source of indistinguishable single photons. The polymers used in this work are also compatible with 1310 nm and 1550 nm light, which opens the possibility of operating such a source at telecom wavelengths. In rubidium atoms, this could be realized by using a transition between the $5P_{1/2}$ and $4D_{3/2}$ states [64]. Furthermore, using multicore fibers it is also possible to integrate arrays of traps into one fiber. In combination with a suitable atomic species, such as strontium, this could be used to realize single-atom clock arrays [14, 15].

Finally, even completely passive vacuum setups are conceivable [65], making these devices fully portable and scalable, and, thus, a promising tool for atomic quantum technologies.

Acknowledgments

We are indebted to Tilman Pfau for generous support and thank Moritz Berngruber, Max Mäusezahl, Kevin Ng, Jan-Niklas Schmidt and Artur Skljarow for technical assistance. This project has received funding from the European Research Council (ERC) under the European Union's Horizon 2020 research and innovation programme (Grant Agreement Nos. 949431 and 862549), Vector Stiftung, the RiSC programme of the Ministry of Science, Research and Arts Baden-Württemberg, Carl Zeiss Foundation, Deutsche Forschungsgemeinschaft (GRK2642), and the Terra Incognita programme of the University of Stuttgart.

Data availability statement

The data that support the findings of this study are available upon reasonable request from the authors.

ORCID iDs

Tim Langen https://orcid.org/0000-0003-2561-0326

References

[1] Ashkin A, Dziedzic J M, Bjorkholm J E and Chu S 1986 Observation of a single-beam gradient force optical trap for dielectric particles *Opt. Lett.* **11** 288–90
[2] Ashkin A 1970 Acceleration and trapping of particles by radiation pressure *Phys. Rev. Lett.* **24** 156–9
[3] Kaufman A M and Ni K-K 2021 Quantum science with optical tweezer arrays of ultracold atoms and molecules *Nat. Phys.* **17** 1324
[4] Bernien H *et al* 2017 Probing many-body dynamics on a 51-atom quantum simulator *Nature* **551** 579–84
[5] de Léséleuc S, Lienhard V, Scholl P, Barredo D, Weber S, Lang N, Büchler H P, Lahaye T and Browaeys A 2019 Observation of a symmetry-protected topological phase of interacting bosons with Rydberg atoms *Science* **365** 775–80
[6] Scholl P *et al* 2021 Quantum simulation of 2D antiferromagnets with hundreds of Rydberg atoms *Nature* **595** 233–8
[7] Ebadi S *et al* 2021 Quantum phases of matter on a 256-atom programmable quantum simulator *Nature* **595** 227–32
[8] Kaufman A M, Lester B J, Foss-Feig M, Wall M L, Rey A M and Regal C A 2015 Entangling two transportable neutral atoms via local spin exchange *Nature* **527** 208–11
[9] Levine H *et al* 2019 Parallel implementation of high-fidelity multiqubit gates with neutral atoms *Phys. Rev. Lett.* **123** 170503
[10] Madjarov I S *et al* 2020 High-fidelity entanglement and detection of alkaline-earth Rydberg atoms *Nat. Phys.* **16** 857–61
[11] Liu L R, Hood J D, Yu Y, Zhang J T, Hutzler N R, Rosenband T and Ni K-K 2018 Building one molecule from a reservoir of two atoms *Science* **360** 900–3

[12] Cheuk L W, Anderegg L, Bao Y, Burchesky S, Yu S S, Ketterle W, Ni K-K and Doyle J M 2020 Observation of collisions between two ultracold ground-state CaF molecules *Phys. Rev. Lett.* **125** 43401

[13] Reynolds L A, Schwartz E, Ebling U, Weyland M, Brand J and Andersen M F 2020 Direct measurements of collisional dynamics in cold atom triads *Phys. Rev. Lett.* **124** 73401

[14] Madjarov I S, Cooper A, Shaw A L, Covey J P, Schkolnik V, Yoon T H, Williams J R and Endres M 2019 An atomic-array optical clock with single-atom readout *Phys. Rev.* X **9** 41052

[15] Young A W, Eckner W J, Milner W R, Kedar D, Norcia M A, Oelker E, Schine N, Ye J and Kaufman A M 2020 Half-minute-scale atomic coherence and high relative stability in a tweezer clock *Nature* **588** 408–13

[16] Thompson J D, Tiecke T G, de Leon N P, Feist J, Akimov A V, Gullans M, Zibrov A S, Vuletić V and Lukin M D 2013 Coupling a single trapped atom to a nanoscale optical cavity *Science* **340** 1202–5

[17] Kim M E, Chang T-H, Fields B M, Chen C-A and Hung C-L 2019 Trapping single atoms on a nanophotonic circuit with configurable tweezer lattices *Nat. Commun.* **10** 1647

[18] Garcia S, Maxein D, Hohmann L, Reichel J and Long R 2013 Fiber-pigtailed optical tweezer for single-atom trapping and single-photon generation *Appl. Phys. Lett.* **103** 114103

[19] Li J *et al* 2020 Ultrathin monolithic 3D printed optical coherence tomography endoscopy for preclinical and clinical use *Light Sci. Appl.* **9** 124

[20] Gissibl T, Thiele S, Herkommer A and Giessen H 2016 Two-photon direct laser writing of ultracompact multi-lens objectives *Nat. Photon.* **10** 554–60

[21] Asadollahbaik A, Thiele S, Weber K, Kumar A, Drozella J, Sterl F, Herkommer A M, Giessen H and Fick J 2020 Highly efficient dual-fiber optical trapping with 3D printed diffractive Fresnel lenses *ACS Photon.* **7** 88–97

[22] Asadollahbaik A, Thiele S, Kumar A, Sterl F, Drozella J, Herkommer A, Heymann M, Fick J and Giessen H 2022 Structured light by 3d printed micro-optical elements enable single fibre optical tweezers (submitted)

[23] Schäffner D, Preuschoff T, Ristok S, Brozio L, Schlosser M, Giessen H and Birkl G 2020 Arrays of individually controllable optical tweezers based on 3D-printed microlens arrays *Opt. Express* **28** 8640–5

[24] Sartison M *et al* 2021 3D printed micro-optics for quantum technology: optimised coupling of single quantum dot emission into a single-mode fibre *Light: Adv. Manuf.* **2** 1

[25] Murr L E 2016 Frontiers of 3D printing/additive manufacturing: from human organs to aircraft fabrication *J. Mater. Sci. Technol.* **32** 987–95

[26] Do A-V, Khorsand B, Geary S M and Salem A K 2015 3d printing of scaffolds for tissue regeneration applications *Adv. Healthcare Mater.* **4** 1742–62

[27] Tay Y W D, Panda B, Paul S C, Mohamed N A N, Tan M J and Leong K F 2017 3d printing trends in building and construction industry: a review *Virtual Phys. Prototyping* **12** 261–76

[28] Saint R *et al* 2018 3D-printed components for quantum devices *Sci. Rep.* **8** 8368

[29] Chen Z *et al* 2019 3d printing of ceramics: a review *J. Eur. Ceram. Soc.* **39** 661–87

[30] Schmid M, Ludescher D and Giessen H 2019 Optical properties of photoresists for femtosecond 3D printing: refractive index, extinction, luminescence-dose dependence, aging, heat treatment and comparison between 1-photon and 2-photon exposure *Opt. Mater. Express* **9** 4564–77

[31] Ristok S, Thiele S, Toulouse A, Herkommer A M and Giessen H 2020 Stitching-free 3D printing of millimeter-sized highly transparent spherical and aspherical optical components *Opt. Mater. Express* **10** 2370–8

[32] Serbin J *et al* 2003 Femtosecond laser-induced two-photon polymerization of inorganic–organic hybrid materials for applications in photonics *Opt. Lett.* **28** 301–3

[33] Deubel M, von Freymann G, Wegener M, Pereira S, Busch K and Soukoulis C M 2004 Direct laser writing of three-dimensional photonic-crystal templates for telecommunications *Nat. Mater.* **3** 444–7

[34] Jiang L J, Maruo S, Osellame R, Xiong W, Campbell J H and Lu Y F 2016 Femtosecond laser direct writing in transparent materials based on nonlinear absorption *MRS Bull.* **41** 975–83

[35] Hahn V, Kiefer P, Frenzel T, Qu J, Blasco E, Barner-Kowollik C and Wegener M 2020 Rapid assembly of small materials building blocks (voxels) into large functional 3D metamaterials *Adv. Funct. Mater.* **30** 1907795

[36] Quero J M, Perdigones F and Aracil C 2018 Microfabrication technologies used for creating smart devices for industrial applications *Smart Sensors and MEMS* ed S Nihtianov and A Luque (Duxford: Woodhead Publishing) pp 291–311

[37] Liu X *et al* 2018 3D printing of bioinspired liquid superrepellent structures *Adv. Mater.* **30** 1800103

[38] Brenner K-H and Singer W 1993 Light propagation through microlenses: a new simulation method *Appl. Opt.* **32** 4984–8

[39] Schmidt S, Thiele S, Herkommer A, Tünnermann A and Gross H 2017 Rotationally symmetric formulation of the wave propagation method-application to the straylight analysis of diffractive lenses *Opt. Lett.* **42** 1612–5

[40] Schlosser N, Reymond G, Protsenko I and Grangier P 2001 Sub-Poissonian loading of single atoms in a microscopic dipole trap *Nature* **411** 1024–7

[41] Grimm R, Weidemüller M and Ovchinnikov Y B 2008 *Adv. At. Mol. Opt. Phys.* **42** 95–170

[42] Steck D A 2008 Rubidium 85 D line data http://steck.us/alkalidata

[43] Ravensbergen C, Corre V, Soave E, Kreyer M, Tzanova S, Kirilov E and Grimm R 2018 Accurate determination of the dynamical polarizability of dysprosium *Phys. Rev. Lett.* **120** 223001

[44] Westergaard P G, Lodewyck J, Lorini L, Lecallier A, Burt E A, Zawada M, Millo J and Lemonde P 2011 Lattice-induced frequency shifts in Sr optical lattice clocks at the 10−17 level *Phys. Rev. Lett.* **106** 210801

[45] Le Kien F, Schneeweiss P and Rauschenbeutel A 2013 Dynamical polarizability of atoms in arbitrary light fields: general theory and application to cesium *Eur. Phys. J.* D **67** 92

[46] Abraham E R I and Cornell E A 1998 Teflon feedthrough for coupling optical fibers into ultrahigh vacuum systems *Appl. Opt.* **37** 1762–3

[47] McGilligan J P *et al* 2020 Laser cooling in a chip-scale platform *Appl. Phys. Lett.* **117** 54001

[48] Burrow O S, Osborn P F, Boughton E, Mirando F, Burt D P, Griffin P F, Arnold A S and Riis E 2021 Stand-alone vacuum cell for compact ultracold quantum technologies *Appl. Phys. Lett.* **119** 124002

[49] Wildermuth S, Krüger P, Becker C, Brajdic M, Haupt S, Kasper A, Folman R and Schmiedmayer J 2004 Optimized magneto-optical trap for experiments with ultracold atoms near surfaces *Phys. Rev.* A **69** 30901

[50] Nshii C C *et al* 2013 A surface-patterned chip as a strong source of ultracold atoms for quantum technologies *Nat. Nanotechnol.* **8** 321–4

[51] Wu X, Zi F, Dudley J, Bilotta R J, Canoza P and Müller H 2017 Multiaxis atom interferometry with a single-diode laser and a pyramidal magneto-optical trap *Optica* **4** 1545
[52] Bowden W, Hobson R, Hill I R, Vianello A, Schioppo M, Silva A, Margolis H S, Baird P E G and Gill P 2019 A pyramid MOT with integrated optical cavities as a cold atom platform for an optical lattice clock *Sci. Rep.* **9** 11704
[53] Gallego D, Hofferberth S, Schumm T, Krüger P and Schmiedmayer J 2009 Optical lattice on an atom chip *Opt. Lett.* **34** 3463–5
[54] Heine D *et al* 2010 A single-atom detector integrated on an atom chip: fabrication, characterization and application *New J. Phys.* **12** 95005
[55] Nirrengarten T, Qarry A, Roux C, Emmert A, Nogues G, Brune M, Raimond J-M and Haroche S 2006 Realization of a superconducting atom chip *Phys. Rev. Lett.* **97** 200405
[56] Bernon S *et al* 2013 Manipulation and coherence of ultra-cold atoms on a superconducting atom chip *Nat. Commun.* **4** 2380
[57] Cantat-Moltrecht T, Cortiñas R, Ravon B, Méhaignerie P, Haroche S, Raimond J M, Favier M, Brune M and Sayrin C 2020 Long-lived circular Rydberg states of laser-cooled rubidium atoms in a cryostat *Phys. Rev. Res.* **2** 022032
[58] Schymik K-N, Pancaldi S, Nogrette F, Barredo D, Paris J, Browaeys A and Lahaye T 2021 Single atoms with 6000-second trapping lifetimes in optical-tweezer arrays at cryogenic temperatures *Phys. Rev. Appl.* **16** 034013
[59] Becker D *et al* 2018 Space-borne Bose–Einstein condensation for precision interferometry *Nature* **562** 391–5
[60] Aveline D C *et al* 2020 Observation of Bose–Einstein condensates in an Earth-orbiting research lab *Nature* **582** 193–7
[61] Altuntaş E, Ammon J, Cahn S B and DeMille D 2018 Demonstration of a sensitive method to measure nuclear-spin-dependent parity violation *Phys. Rev. Lett.* **120** 142501
[62] Kogel F, Rockenhäuser M, Albrecht R and Langen T 2021 A laser cooling scheme for precision measurements using fermionic barium monofluoride ($^{137}Ba^{19}F$) molecules *New J. Phys.* **23** 095003
[63] Madkhaly S H, Coles L A, Morley C, Colquhoun C D, Fromhold T M, Cooper N and Hackermüller L 2021 Performance-optimized components for quantum technologies via additive manufacturing *PRX Quantum* **2** 30326
[64] Uphoff M, Brekenfeld M, Rempe G and Ritter S 2016 An integrated quantum repeater at telecom wavelength with single atoms in optical fiber cavities *Appl. Phys.* B **122** 46
[65] Rushton J A, Aldous M and Himsworth M D 2014 Contributed review: the feasibility of a fully miniaturized magneto-optical trap for portable ultracold quantum technology *Rev. Sci. Instrum.* **85** 121501